

---

# Optimum Processing Protocols for Volume Determination of the Liver and Spleen from SPECT Imaging with Technetium-99m Sulfur Colloid

Fernando Mut, Steve Glickman, Donna Marciano, and Randall A. Hawkins

*Division of Nuclear Medicine and Biophysics, Department of Radiological Sciences, UCLA School of Medicine, Los Angeles, California*

A study of the effects of processing parameters on the determination of liver and spleen volume from SPECT data was performed. A method for volume determination using a threshold algorithm was calibrated against phantoms and applied to 60 patient studies. Good reproducibility was found using different projections and computing the volume on separate days. Variations of the measured volumes with the threshold value, reconstruction filter cutoff frequency and attenuation correction were investigated. Reconstruction parameters producing best image quality were also determined. A threshold of 25% of the maximum value in the organ was determined from phantom studies. Changes of 1% around this value yielded changes of 2–3% in the computed volume. No significant change was noted as cutoff frequencies varied between 0.4 and 0.85 of Nyquist (0.031 to 0.066 cycles/cm) for a third order Butterworth filter. Attenuation correction produced a decrease of 9% and 6% in liver and spleen measured volume respectively. Best image quality was obtained with 0.4 Nyquist (0.031 cycles/cm) cutoff frequency for third order Butterworth filter and attenuation correction. It is concluded that optimal parameters must be determined for any processing protocol, and must then be adhered to in future applications to insure clinical accuracy, especially those parameters demonstrating the most quantitative and qualitative sensitivity.

J Nucl Med 29:1768–1775, 1988

---

One of the applications of single photon emission computed tomography (SPECT) is in the evaluation of the liver and spleen with technetium-99m [<sup>99m</sup>Tc]sulfur colloid. In addition to a higher sensitivity for lesion detection compared with planar scintigraphy (1,2), SPECT provides the opportunity to measure organ volumes (3–12). We investigated the effects of several processing parameters on the determination of liver and spleen volume from SPECT data, and on the subjective quality of the images.

## MATERIALS AND METHODS

### Algorithm for Volume Determination

A relatively simple semiautomated method was developed to measure organ volume, based on the reconstructed cross-

sectional images. Volumes were measured by determining the boundary of the object in each slice, determining the area from the number of pixels within the boundary, and adding these areas to yield the result.

To determine the boundary of the object in each slice, the following algorithm was used.

All transverse slices spanning the object are added pixel-by-pixel to form a sum image. The operator is prompted to draw a boundary on this sum image enclosing the object. This boundary serves two purposes. First, the pixels it encloses define a mask to be applied to each slice in subsequent steps. Second, the pixels on the sides of the smallest rectangle enclosing this boundary, in each slice, are used to determine neighborhood values through bilinear interpolation, to be subtracted from pixels within the boundary to suppress possible distortions due to reconstruction effects. If this rectangle is observed to intersect any region where the intensity due to uptake, rather than artifact, is more than a fraction of a percent of the intensity in the organ, the operator can bypass this correction, or choose another orientation.

The operator is prompted to select a threshold value, as a percentage of maximum pixel value in slices in the masked

---

Received June 29, 1987; revision accepted June 27, 1988.

For reprints contact: Randall A. Hawkins, MD, PhD, Div. of Nuclear Medicine and Biophysics, Dept. of Radiological Sciences, UCLA School of Medicine, Los Angeles, CA 90024.

region, to be used to define the boundary in each slice image. The algorithm then automatically defines and draws a boundary around the object in each transverse slice where it appears. The images are then displayed with the object boundary superimposed and the operator has the option of correcting any boundary, either by manual drawing or selecting a new threshold value. When the operator considers all the boundaries to be correct, the enclosed voxels are summed, scaled by the voxel size, and the resulting value for the object volume in cubic centimeters is displayed.

#### Determination of Pixel Size

A  $^{99m}\text{Tc}$  point source was placed in the center of the detector, and at eight additional points at known distances from the center; four on the x and y axes and four at  $45^\circ$ . Images were acquired with 5,000 total counts for each position of the point source using a  $64 \times 64 \times 16$  matrix. The position of the point was determined from the centroid of the counts. Measured distances between the point sources were compared with the distances in pixels to obtain the pixel size.

#### Phantom Studies

To validate the method, a latex phantom was filled with water and 5 mCi (0.2 GBq) of [ $^{99m}\text{Tc}$ ]pertechnetate. The phantom was enclosed in a hollow plastic cylinder filled with water and held in position with tape (Fig. 1). Volumes of 500, 1,000, 1,500 cc were used, measured both by displacement and weight, which agreed to better than 1%. Imaging was performed with the axis of the cylinder coincident with the axis of rotation of the camera and repeated studies were made at all volumes, rotating or reversing the cylinder, and on different days (Table 1).

All studies were acquired using a Siemens Orbiter LFOV rotating gamma camera with a low-energy, all purpose collimator and connected on line with a Siemens Microdelta computer system.

A  $64 \times 64 \times 16$  matrix was used and data were acquired over  $360^\circ$  in 64 angular steps, for 10 sec per view. Reconstruction of cross-sectional images was done by filtered backprojec-

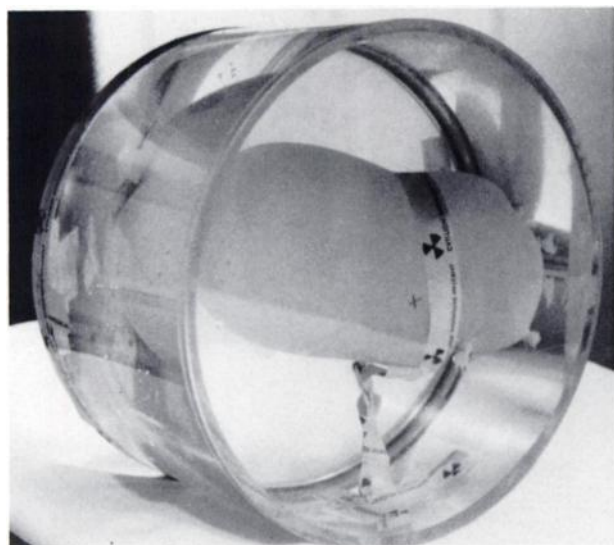


**FIGURE 1**  
The phantom used for calibration.

**TABLE 1**  
Phantom Volume Measurements Computed Volume (cc)

True volume	Day 1		Day 2
	Position A	Position B	Position A
500	495	481	489
1,000	974	1,019	967
1,500	1,466	1,467	1,414

tion, using a third order Butterworth window with a cutoff at 0.70 of the Nyquist frequency (0.054 cycles/cm) on the ramp filter. No attenuation correction was performed. Sagittal and coronal slices were generated from the transverse reconstructed images.

Volume calculation was performed for all phantom studies on the transverse, sagittal and coronal slices using different thresholds to determine the threshold yielding the closest result to the true volume.

#### Patient Studies

Subsequently, 60 patients were studied who were referred to the UCLA Nuclear Medicine Clinic for liver-spleen evaluation. Five to six millicuries (0.2 GBq) of [ $^{99m}\text{Tc}$ ]sulfur colloid were administered intravenously to each patient, and acquisition started 15 min later, using the same instruments as described for the phantom studies. Acquisition parameters were similar to those for the phantom studies, except that the imaging time was 20 sec per view. Anterior and right lateral planar reference images were also obtained. Reconstruction was done in a manner identical to that used for the phantom studies. Additional sets of images were generated by reconstructing the studies of three patients using cutoff frequencies of 1.0, 0.85, 0.70, 0.55, 0.40, 0.25 and 0.10 Nyquist (0.077, 0.066, 0.054, 0.043, 0.031, 0.014, 0.008 cycles/cm).

After volume calculation of the liver and spleen from the transverse slices, attenuation correction was performed using the method proposed by Chang (13).

In ten cases, the volume computation was also done from the sagittal and coronal slices to determine the reproducibility of the method using different slice orientations (Fig. 2 and Table 2).

We also measured the liver and spleen volume in three patients from transverse slices reconstructed with seven different cutoff frequencies and in ten studies with and without attenuation correction in order to assess the influence of these parameters on the quantitative results and on the quality of the images.

Using the threshold determined from phantom studies, the variation in calculated volume with small changes around this value was investigated by re-running the algorithm on the liver and spleen images of five patients, varying the threshold in 2% increments.

Finally, the intraobserver reproducibility was tested by computing the liver and spleen volumes of ten patients on two different occasions, several days apart. No interobserver reproducibility was explored.

## RESULTS

The pixel size using a  $64 \times 64$  matrix was found to be 6.47 mm, giving a voxel volume of 0.27 cc.

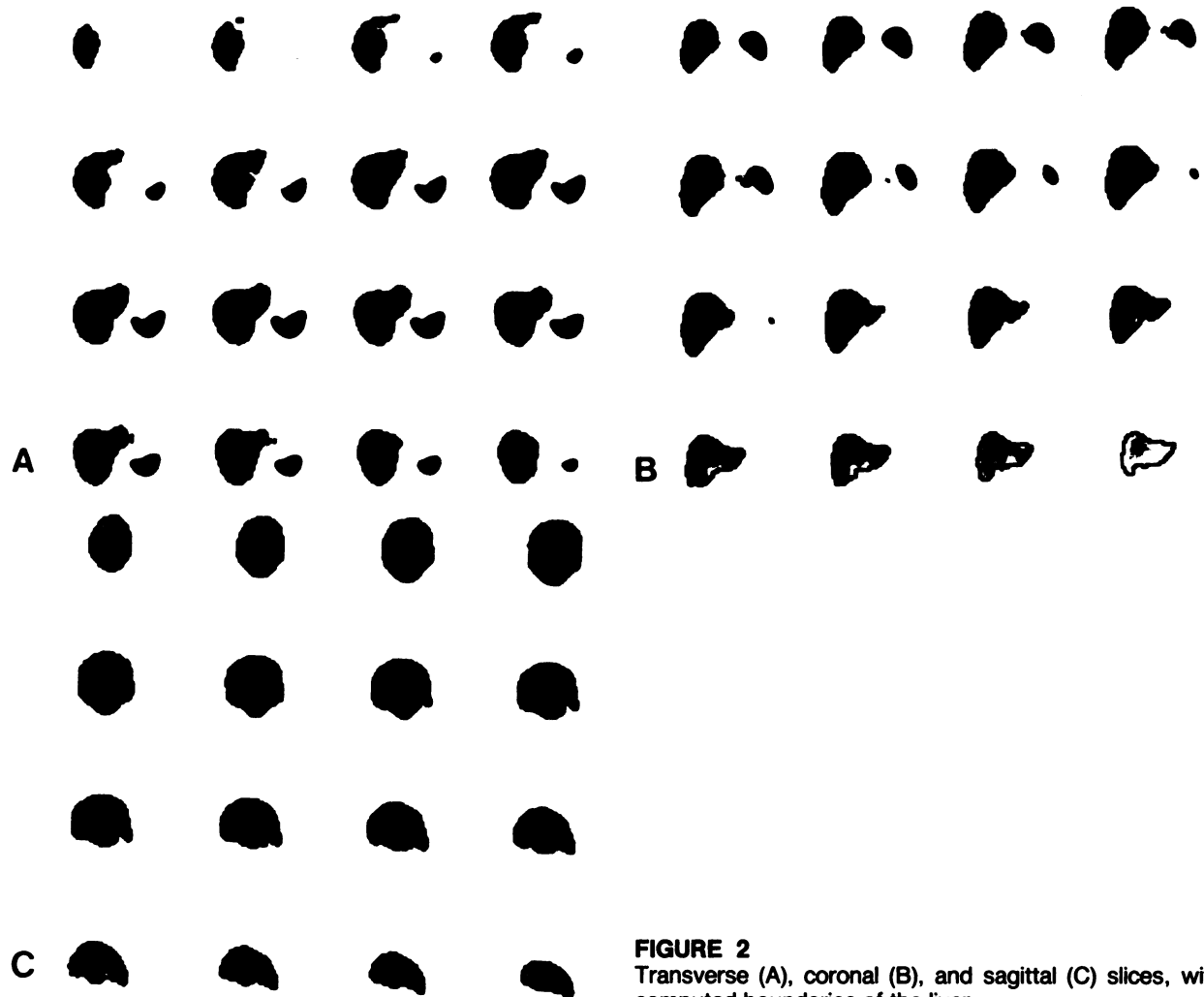


**FIGURE 2**  
Transverse (A), coronal (B), and sagittal (C) slices, with computed boundaries of the liver.

Thresholds yielding volumes equal to the known phantom volumes were 24.4%, 25.03%, and 24.63% for the 500 cc, 1,000 cc, and 1,500 cc phantoms, respectively (Fig. 3). Thus, a general threshold of 25% was defined, which gave a mean error of 2.85% on volume computation.

The measured volume was found to be more sensitive to variation in the threshold than in any other parameter investigated. We observed changes of 2% to 3% in calculated liver and spleen volume with 1% change in threshold in the region of the nominal 25% value determined from phantom studies (Fig. 4).

Figure 5 illustrates the accuracy of the technique, and the expected insensitivity of a thresholding technique to slice orientation. Phantom values measured using the same data arranged in transverse, coronal, and sagittal slices are plotted against the known values in Figure 5A, showing a variation with orientation of 4%. The same analysis applied to clinical data, seen in Figure 5B, shows a 5% variation.

Analyzing the data from two different measurements of the liver and spleen volume on ten patients made by

the same operator several days apart demonstrated a mean difference of 2.28%.

The decrease in percent error with increasing volume is consistent with a constant error in the radial, or normal direction. Given the cubic variation of calculated volume with this dimension, the percent error in the volume is expected to vary inversely as the cube root of the volume.

Subjective evaluation of studies from patients known to have liver disease, or to be normal, (from diagnosis based upon other diagnostic procedures including liver tests, CT, US, MRI, and liver biopsy reconstructed with different filter cutoffs) demonstrated that the 0.4 Nyquist (0.31 cycles/cm) cutoff value of the third order Butterworth filter produced the best image quality (Fig. 6). Lower cutoff frequencies provided over-smoothed data affecting the image resolution, whereas higher frequencies allowed statistical noise to produce the impression of mottled uptake and irregular edges in the organs under study.

These two situations lead to a decrease in the diagnostic accuracy of the method, since they tend to pro-

**TABLE 2**  
Measured Volume from Orthogonal Slices

	Transverse (cc)	Coronal (cc)	Sagittal (cc)
<b>Phantoms</b>			
500 cc	495	479	522
1,000 cc	974	960	955
1,500 cc	1466	1469	1472
<b>Patients organ<sup>a</sup></b>			
1 (L)	2,017	2,020	2,004
(S)	293	295	294
2 (L)	1,327	1,331	1,334
(S)	334	367	362
3 (L)	1,483	1,487	1,492
(S)	321	342	340
4 (L)	1,190	1,183	1,158
(S)	213	203	198
5 (L)	1,118	1,147	1,067
(S)	166	163	175
6 (L)	1,554	1,507	1,498
(S)	167	161	165
7 (L)	1,566	1,618	1,560
(S)	258	262	268
8 (L)	1,050	1,013	1,062
(S)	335	317	367
9 (L)	1,789	1,805	1,764
(S)	383	354	364
10 (L)	1,213	1,223	1,182
(S)	284	273	284

<sup>a</sup>(L) Liver; (S) Spleen.

duce false-negative results in the former case and false-positive ones in the latter.

The volume calculation showed no significant difference using filter cutoff frequencies between 0.4 and 0.85, Nyquist (0.31 and 0.66 cycles/cm) whereas a significant change occurred at 0.25 and 0.1, Nyquist (0.19 and 0.08 cycles/cm) and a less dramatic change above 0.85 (Fig. 7). Spleen-to-liver volume ratios showed that the spleen volume was proportionally more affected by the cutoff value than was the liver, particularly at 0.1 Nyquist (0.08 cycles/cm) (Fig. 8).

Comparing the values obtained from attenuation corrected and noncorrected images, we found a mean difference of 9.15% for the liver volume and 5.82% for the spleen volume, in both cases lower for the attenuation corrected studies (Table 3).

As seen in the example in Figure 9, reconstruction artifacts, possibly due to partial volume effects, sometimes connect the organ being processed to nearby intense structures. If the reconstructed pixel values in such an artifact reach the threshold, the boundary defined by the algorithm in the affected slices will be distorted, as seen in Figure 9A, and the contribution to the organ volume from these slice areas will be incorrectly increased.

To selectively and automatically suppress this distortion if it occurs without changing the rest of the bound-

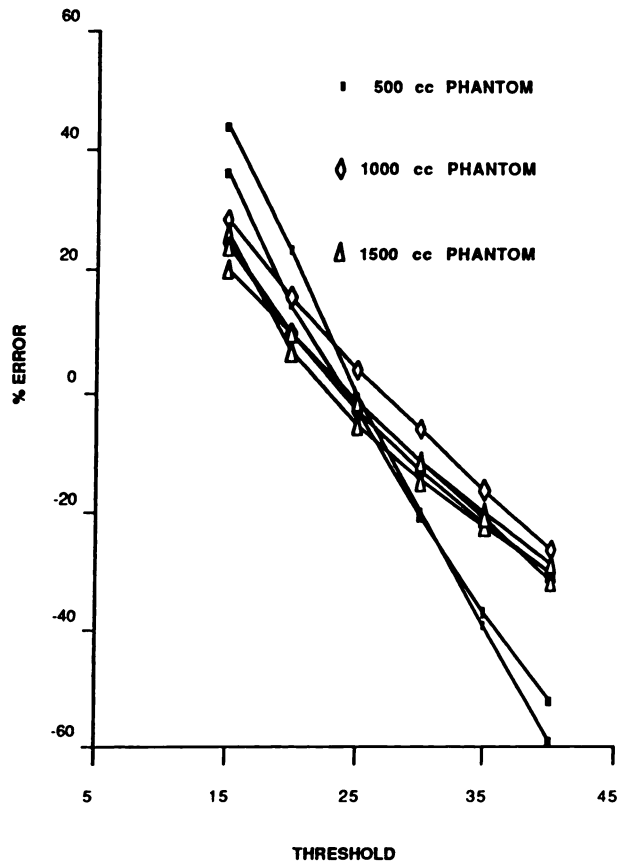


**FIGURE 3**  
Variation in measured phantom volume with threshold.

ary, we applied a correction by subtracting values interpolated from the rectangle enclosing the mask, seen in Figure 9B. The new boundary computed after subtracting the correction image is seen in Figure 9C. The correction image from the interpolation is seen in Figure 9D.

In regions outside intense objects where no such artifacts are present, the reconstructed pixel values are typically <0.1% of those inside the organ so that this operation, as desired, has no effect on the adjacent calculated boundary, as can be seen by comparing Figure 9A to Figure 9C.

## DISCUSSION

Our threshold of 25% for the phantom studies is considerably lower than that found by other authors. Kodama et al. (11) propose a 35% threshold, while Tauxe et al. (6) as well as Soderborg et al. (8), worked with a 45–46% value. Kawamura et al. (10) report that the volume of kidney phantoms ranging from 100 cc to 430 cc was best predicted using a 51% threshold. These differences in optimal threshold for volume calculation may be explained by the fact that the above-mentioned investigators all used different pre- and post-

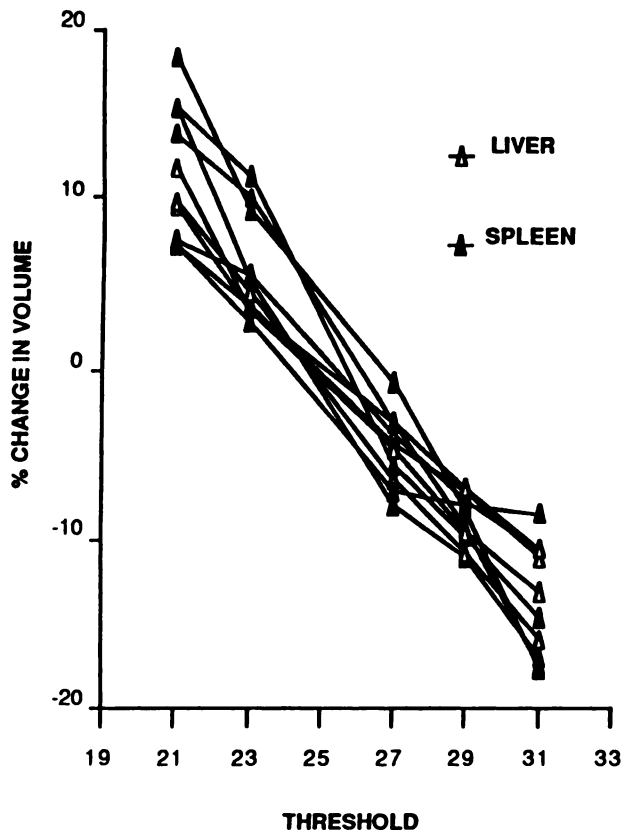


**FIGURE 4**  
Variation in measured organ volume with threshold.

processing procedures. As we demonstrated and will discuss later, different data processing yields different quantitative results for a given threshold, thus the optimal threshold value is dependent on the type of processing employed (12).

The mean error of 2.8% for the phantom studies is lower than that reported by Strauss et al. (9) and Kan et al. (3), who found an absolute error of 3.4% and

7.2%, respectively. Given that a 1,000 cc object would comprise ~4,000 voxels with a 1,500 pixel surface area, we consider this accuracy to be encouraging. It must be noted that for the present study, however, only three different volumes were measured with the smallest being 500 cc.

Good reproducibility was found in repeated measurements made by repositioning the phantom either on the same day or on different days, demonstrating stable field uniformity of the camera.

As reported by other authors (6,7), no significant difference was found between calculations using the transverse, coronal, or sagittal slices, either on the phantom or the patient studies.

Good intraobserver reproducibility was demonstrated by one operator performing two different measurements on the same ten patient studies several days apart. Further investigation is needed to determine the interobserver reproducibility of the method.

For the patient studies, we found a 0.4 Nyquist (0.31 cycles/cm) cutoff frequency of the third order Butterworth filter to produce a high quality image without a significant alteration of the volume measurement results. In fact, the results using different cutoff frequencies demonstrated no important variation between 0.4 and 0.85, Nyquist (0.31 and 0.66 cycles/cm) although the computed volume tends to display an inverse relationship with the cutoff values. This is consistent with widening of the point spread function at lower cutoff values causing the boundary of the organ, as defined by the algorithm, to be outside the true boundary. Higher cutoff frequencies cause the algorithm to construct a boundary closer to the true one, since the point spread function becomes narrower, but qualitatively degrade the images due to the presence of random noise (Fig. 6).

Thus, a compromise must be reached between a reasonably accurate volume measurement and a rea-

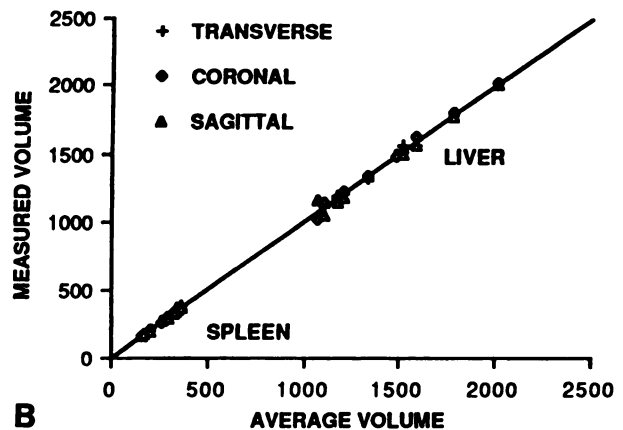
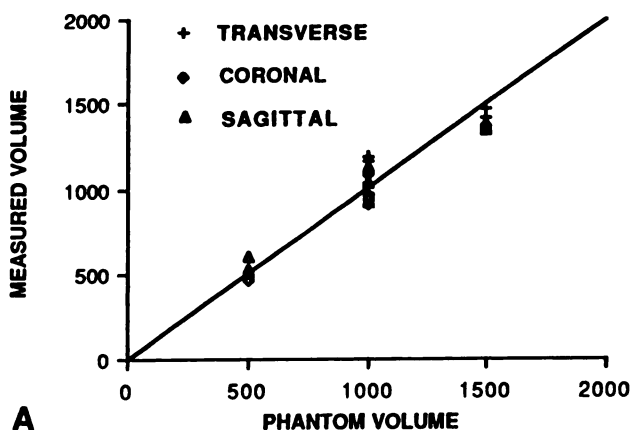


**FIGURE 5**  
Measured volume from transverse, coronal, and sagittal slices vs. (a) known phantom volume and (b) average of the three measurements.

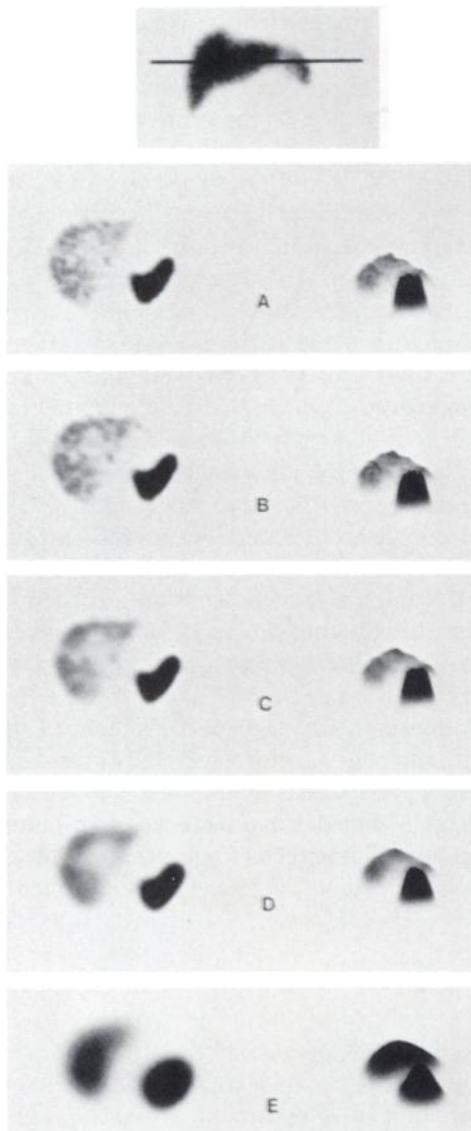


**FIGURE 6**  
One transverse slice from a normal liver, reconstructed with cutoff frequencies of (A) 1.0, (B) 0.7, (C) 0.4, (D) 0.25, (E) 0.1. Intensity on right, two-dimensional histogram on left.

sonably noise-free image in order to achieve good diagnostic accuracy.

Likewise, spatial smoothing of the data either before or after reconstruction causes the calculated volume to be overestimated. As noted before, this may explain the differences among optimal threshold values that different authors propose for volume calculation.

We observed that the algorithm calculated a lower volume when attenuation correction was applied to the images. As Malko et al. pointed out (14), since algorithms employing a threshold technique in which the count level of each pixel is used to decide whether the pixel is to be included in the calculated volume, any modification of the pixel count level may affect the result. The algorithm defines the boundary of the organ

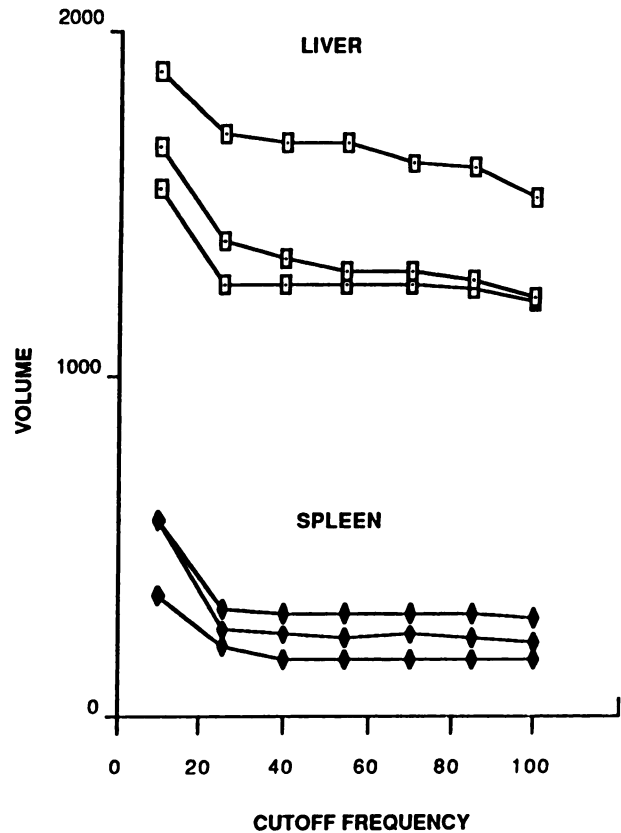


**FIGURE 7**  
Liver and spleen volume vs. cutoff frequency as percent of Nyquist.

in each slice by comparing pixels near the edge of the organ with the pixel in the organ having the highest value. This maximum pixel is usually deep within the organ. The attenuation correction algorithm typically increases the value of such internal pixels relatively more than pixels on the organ boundary, which are closer to the body boundary. The net effect of raising

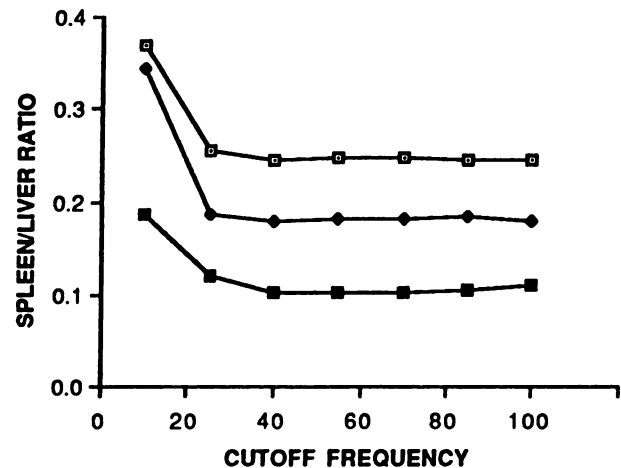


**FIGURE 8**  
Spleen-to-liver volume ratio vs. cutoff frequency as percent of Nyquist.

**TABLE 3**  
Measured Organ Volume With and Without Attenuation Correction

Patient no.	Liver			Spleen		
	N/C* (cc)	C† (cc)	% Diff.	N/C (cc)	C (cc)	% Diff.
1	1,268	1,216	4.10	152	142	6.58
2	1,324	1,293	2.34	237	216	8.86
3	2,296	1,973	14.07	360	337	6.39
4	2,095	1,839	12.22	945	907	4.02
5	1,397	1,215	13.03	2,250	2,177	3.24

\* N/C = not corrected for attenuation.  
† C = corrected for attenuation.

the relative value of the maximum pixel is to effectively raise the threshold, which shrinks the calculated boundary, and hence the computed volume.

Difficulties with automatic edge definition were found in some patients. Space-occupying lesions within the liver parenchyma caused the algorithm to underestimate the actual liver volume since the lesion volume was excluded from the total organ volume. This can be overcome by re-running the algorithm on the lesion as a separate object, manually drawing the outline of the lesion, which will typically be limited to four or five

slices, thus obtaining the lesion's volume, which can be added to the computed liver volume to obtain the total organ volume. This procedure provides additional useful clinical information on the lesion volume which can be recorded as a base-line for follow-up purposes.

Left lobe overlap into the spleen is a usual finding even in the absence of left lobe hypertrophy. This normal variant constitutes a common pitfall for automatic edge-detection. In our experience this problem can be solved in most cases by using either the coronal or the sagittal projection since a separation between both organs will usually be observed in at least one of these projections.

Very intense bone marrow uptake is another source of error. Because this finding usually occurs in advanced liver disease, the liver most probably will be reduced in size and sufficient separation from the surrounding skeleton will exist. However, overlapping can still occur, causing the automatic edge detection algorithm to include some neighboring structures such as the sternum. Again, use of different projections may overcome this problem.

Lung uptake of the radiocolloid is a less common source of error, but when it exists and is close enough to the liver uptake it may be impossible to separate the two organs. Although we had no cases in our series, kidney uptake could potentially lead to a similar problem.

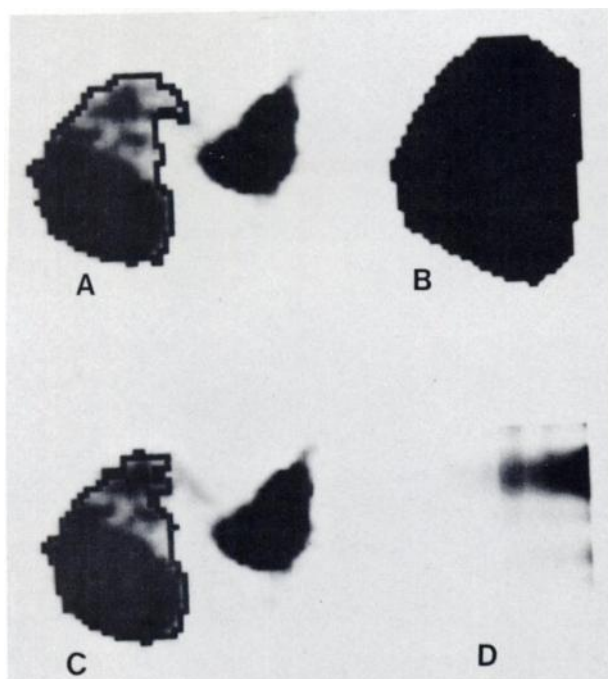


**FIGURE 9**  
Suppression of reconstruction artifacts. (A) Liver with the modified boundary distorted by artifact connecting to adjacent spleen. (B) The mask used to define the liver and the rectangle for the interpolation correction. (C) The liver with the modified boundary after correction. (D) The intensity generated by the interpolation.

## CONCLUSIONS

As more technology is involved in producing a diagnostic result, more variables are introduced whose modifications could affect that result. We have investigated the effects of different processing parameters on some qualitative and quantitative aspects of liver and spleen SPECT studies. Our investigation of one method of quantitating SPECT data leads to the following general conclusions.

1. Each such method must be validated, and parameters calibrated, against known standards.
2. Once optimal parameters and techniques have been determined for a given method, they must be adhered to in future applications to insure clinical precision and accuracy, with particular attention given to those parameters demonstrating the most quantitative and qualitative sensitivity.

## ACKNOWLEDGMENTS

The authors thank Dr. L. R. Bennett for his support, Autumn Anderson and Chris Carlson for their assistance in processing the studies, the staff of the UCLA Nuclear Medicine Clinic, and Maggie Marquez and Robin Boynton for typing the manuscript.

## REFERENCES

1. Jaszczak R, Whitehead F, Lim D, et al. Lesion detection with single-photon emission computed tomography (SPECT) compared with conventional imaging. *J Nucl Med* 1982; 23:97-102.
2. Strauss L, Bostel F, Clorius J, et al. Single-photon emission computed tomography (SPECT) for assessment of hepatic lesions. *J Nucl Med* 1982; 23:1059-1065.
3. Kan M, Hopkins GB. Measurement of liver volume by emission computed tomography. *J Nucl Med* 1979; 20:514-520.
4. Shapiro B, Rigby L, Britton K. The assessment of thyroid volume with single photon emission tomography. *Nucl Med Commun* 1980; 1:33-36.
5. Gustafsson H. Volume determination by emission computed tomography (ECT) of radionuclide distributions. Thesis, Karolinska Institute, Stockholm, RI 1982-01, 1982.
6. Tauxe WN, Soussaline F, Todd-Pokropek A, et al. Determination of organ volume by single-photon emission tomography. *J Nucl Med* 1982; 23:984-987.
7. Tauxe WN, Todd-Pokropek A, Soussaline F, et al. Estimates of kidney volume by single-photon emission tomography: a preliminary report. *Eur J Nucl Med* 1983; 8:72-74.
8. Soderborg B, Dahlbom M, Karlberg N, et al. Determination of organ volume by single-photon emission tomography [Letters to the Editor]. *J Nucl Med* 1983; 24:1197.
9. Strauss L, Clorius J, Frank T, et al. Single-photon emission computerized tomography (SPECT) for estimates of liver and spleen volume. *J Nucl Med* 1984; 25:81-85.
10. Kawamura J, Itoh H, Yoshida O, et al. In vivo estimation of renal volume using a rotating gamma camera for <sup>99m</sup>Tc-dimercaptosuccinic acid renal imaging. *Eur J Nucl Med* 1984; 9:168-172.
11. Kodama T, Watanabe K, Hoshi H, et al. Diagnosis of diffuse hepatocellular diseases using SPECT. *J Nucl Med* 1986; 27:616-619.
12. Mortelmaus L, Nuyts J, Van Pamel G, et al. A new thresholding method for volume determination by SPECT. *Eur J Nucl Med* 1986; 12:284-290.
13. Chang LT. A method for attenuation correction in radionuclide computed tomography. *IEEE Trans Nucl Sci* 1978; NS-25:638-643.
14. Malko J, Van Heertum R, Gullberg G, et al. SPECT liver imaging using alternative attenuation correction algorithm and an external flood source. *J Nucl Med* 1986; 27:701-705.